On the vacuum Einstein equations along curves with a discrete local rotation and reflection symmetry

JCAP08(2015)025

(http://iopscience.iop.org/1475-7516/2015/08/025)

Journal of Cosmology and Astroparticle Physics
An IOP and SISSA journal

On the vacuum Einstein equations along curves with a discrete local rotation and reflection symmetry

Mikołaj Korzyński,[a] **Ian Hinder**[b] **and Eloisa Bentivegna**[c,d]

[a]Center for Theoretical Physics, Polish Academy of Sciences,
Al. Lotników 32/46, Warsaw, 02-668 Poland
[b]Max-Planck-Institut für Gravitationsphysik, Albert-Einstein-Institut,
Am Mühlenberg 1, Golm, D-14476 Germany
[c]Dipartimento di Fisica e Astronomia, Università degli Studi di Catania,
Via S. Sofia 64, Catania, 95123 Italy
[d]INFN, Sezione di Catania,
Via S. Sofia 64, Catania, 95123 Italy

E-mail: korzynski@cft.edu.pl, ian.hinder@aei.mpg.de, eloisa.bentivegna@ct.infn.it

Received May 28, 2015
Accepted July 9, 2015
Published August 13, 2015

Abstract. We discuss the possibility of a dimensional reduction of the Einstein equations in S^3 black-hole lattices. It was reported in previous literature that the evolution of spaces containing curves of local, discrete rotation and reflection symmetry (LDRRS) can be carried out via a system of ODEs along these curves. However, 3+1 Numerical Relativity computations demonstrate that this is not the case, and we show analytically that this is due to the presence of a tensorial quantity which is not suppressed by the symmetry. We calculate the term analytically, and verify numerically for an 8-black-hole lattice that it fully accounts for the anomalous results, and thus quantify its magnitude in this specific case. The presence of this term prevents the exact evolution of these spaces via previously-reported methods which do not involve a full 3+1 integration of Einstein's equation.

Keywords: cosmological simulations, gravity, GR black holes

ArXiv ePrint: 1505.05760

doi:10.1088/1475-7516/2015/08/025

JCAP08(2015)025

Contents

1 S^3 black-hole lattices and dimensional reduction

Black hole lattices, and in particular those conformally related to the 3-sphere S^3, have recently been the object of several studies [1–6] serving as toy models for the evolution of inhomogeneous universes [2, 3], for the propagation of gravitational waves in periodic spaces [4], for the exploration of cosmological models of non-trivial topology [5], and as an application of Regge calculus [6].

In [3], in particular, it was pointed out that the existence of a time-symmetric spatial hypersurface in these models, in addition to the high degree of spatial symmetry of the cell edges, implied that the evolution of the proper length of these subspaces was governed by a system of ordinary differential equations, and was thus decoupled from the surrounding spacetime. Here, however, we show that this is not the case: the symmetry is not sufficient to suppress one term, proportional to the curl of the magnetic part of the Weyl tensor, which contains spatial derivatives of the extrinsic curvature, and therefore prevents the reduction of the evolution equations to a simple, localized ODE system.

In section 2, we present the arguments of [3] and the corresponding ODE system. In section 3, we integrate the Einstein equations numerically in 3+1 dimensions, and show that the comparison between the result and the solution of the ODE system features an anomaly which converges to a non-zero value in the continuum limit. In section 4, we rederive the equations of motion of S^3 black-hole lattices on the cell edges, and illustrate the origin of the curl term. We also show that in the 8-black-hole case, the additional term initially vanishes together with its first two time derivatives, but its third time derivative does not,

JCAP08(2015)025

thus providing the final piece of evidence that the ODE system from [3] does not hold for the 8-black-hole lattice. Finally, we show in section 5 that the anomaly measured numerically in section 3 coincides with the curl term derived in section 4, and provide a fitting formula for representing this term analytically, so that the ODE system can still be used in combination with this source term. We provide some conclusions in section 6.

We will use the following index conventions throughout the paper: Greek indices μ, ν, ..., will run from 0 to 3 and denote the spacetime objects. Objects defined on a spatial slice of dimension 3 will be denoted using Latin indices i, j, ... Tensorial quantities will be sometimes written in the index notation (γ_{ij}, K_{ij}) and sometimes in the index-free notation using the bold typeface $\boldsymbol{\gamma}$, $\mathbf{K}$.

2 Definition and properties of the LDRRS curves

In this section we will introduce the mathematical formalism required to formulate the result of this paper. We will first restate the definition of a curve with a local, discrete rotation and reflection symmetry (LDRRS), discuss the effects of these symmetries and present the ODEs derived in [3]. The derivation of the reduced Einstein equations in [3] has been performed using the orthonormal frame approach in the version given by van Elst and Uggla [7]. This approach is less known than the standard ADM formalism and certainly less useful in numerical investigations where we have direct access to the 3-metric and the extrinsic curvature on a time slice, rather than the Ricci rotation coefficients or the commutation relations of an orthonormal frame. We shall therefore present here the derivation of the reduced evolution equations from the ADM equations. Naturally, the final result does not depend on the formalism used.

Consider the vacuum ADM equations in the normal gauge (corresponding to Gaussian normal coordinates, shift $\beta^i = 0$, lapse $\alpha = 1$)

$$\dot{\gamma}_{ij} = -2K_{ij} \tag{2.1}$$
$$\dot{K}_{ij} = R_{ij} - 2K_{ik}\,K^{k}{}_{j} + K\,K_{ij}\,, \tag{2.2}$$

where γ_{ij} is the 3-metric on a spacelike hypersurface Σ, K_{ij} denotes the extrinsic curvature of this hypersurface, $K = K^{i}{}_{i}$ its trace and R_{ij} is the 3-dimensional Ricci tensor of γ_{ij}. The constraint equations read

$$R + K^2 - K_{ij}\,K^{ij} = 0 \tag{2.3}$$
$$\left(K^{ij} - K\,\gamma^{ij}\right)_{;i} = 0\,, \tag{2.4}$$

where $R = R^{i}{}_{i}$ and the covariant derivative is taken with respect to γ_{ij} [8–10].

Following [3], we assume that on a given Σ there exists a curve λ and a discrete group of symmetries G in the form of discrete n-fold rotations about λ together with reflections through planes passing through λ. More precisely, we assume that for each $a \in G$ there exists a mapping R_a defined on a neighbourhood of λ which preserves both the 3-metric and the extrinsic curvature:

$$R_a^*\,\boldsymbol{\gamma} = \boldsymbol{\gamma}$$
$$R_a^*\,\mathbf{K} = \mathbf{K},$$

R_a^* denoting the pullback of a tensor by R_a. We assume it leaves every point in λ invariant:

$$R_a(p) = p \qquad \text{if} \quad p \in \lambda.$$

JCAP08(2015)025

It follows from the assumptions above that R_a induces a mapping on the tangent space at every point $p \in \lambda$, i.e. $R_a^* : T_p\Sigma \mapsto T_p\Sigma$, which leaves both γ_{ij} and K_{ij} at p invariant.

We also assume that the action of G on $T_p\Sigma$ is the action of the group of discrete rotations and reflections. This assumption may be phrased in the following way: let r generate the rotations and let m and r generate the reflections. Then, in an appropriately chosen, properly oriented orthonormal frame $\mathbf{e}_i$ in $T_p\Sigma$, we have

$$R_r^*(\mathbf{e}_1) = \mathbf{e}_1 \tag{2.5}$$

$$R_r^*(\mathbf{e}_2) = \cos\frac{2\pi}{n}\,\mathbf{e}_2 + \sin\frac{2\pi}{n}\,\mathbf{e}_3 \tag{2.6}$$

$$R_r^*(\mathbf{e}_3) = -\sin\frac{2\pi}{n}\,\mathbf{e}_2 + \cos\frac{2\pi}{n}\,\mathbf{e}_3 \tag{2.7}$$

and

$$R_m^*(\mathbf{e}_1) = \mathbf{e}_1 \tag{2.8}$$

$$R_m^*(\mathbf{e}_2) = -\mathbf{e}_2 \tag{2.9}$$

$$R_m^*(\mathbf{e}_3) = \mathbf{e}_3\,, \tag{2.10}$$

where $\mathbf{e}_1$ has been chosen to be tangent to λ. Note that $\mathbf{e}_1$, $\mathbf{e}_2$ and $\mathbf{e}_3$ are not coordinate basis vectors.

It is straightforward to see that the time development of λ under the vacuum Einstein equations in normal coordinates will be a curve with local rotation and reflection symmetry. In [3] the authors prove that the assumption of invariance under (2.5)–(2.10) restricts the form of vectors and tensors at points lying on λ. In particular, a vector field X^i invariant with respect to rotation (2.5)–(2.7) has to be aligned along the curve λ at every point $p \in \lambda$:

$$\mathbf{X}_p = X_1\,\mathbf{e}_1 \tag{2.11}$$

and every rotation-invariant symmetric 2-tensor $S_{ij} = S_{(ij)}$ is a combination of the metric and a symmetric traceless tensor:

$$\mathbf{S}_p = \frac{S^i{}_i}{3}\,\boldsymbol{\gamma} + S_{11}\left(\boldsymbol{\alpha}_1 \otimes \boldsymbol{\alpha}_1 - \frac{1}{2}\boldsymbol{\alpha}_2 \otimes \boldsymbol{\alpha}_2 - \frac{1}{2}\boldsymbol{\alpha}_3 \otimes \boldsymbol{\alpha}_3\right), \tag{2.12}$$

where $S^i{}_i$ is the trace of S, S_{11} is the $(1,1)$ component of S_{ij} in the orthonormal frame $\mathbf{e}_i$ and $\boldsymbol{\alpha}^i$ is the dual co-frame of $\mathbf{e}_i$, i.e. $\boldsymbol{\alpha}^i(\mathbf{e}_j) = \delta^i{}_j$. On the other hand, every rotation- and reflection-invariant antisymmetric 2-tensor $A_{ij} = A_{[ij]}$ has to vanish at p:

$$\mathbf{A}_p = 0. \tag{2.13}$$

It follows quite easily from (2.11) that λ must be a geodesic with respect to γ_{ij}. Indeed, let $\mathbf{v}$ be a tangent vector to λ in any parametrization. The vector $\nabla_{\mathbf{v}}\mathbf{v}$ is rotation-invariant since both the curve λ and the metric γ_{ij} are invariant as well. From (2.11) it must be proportional to $\mathbf{e}_1$, and thus also to $\mathbf{v}$ itself. After a suitable reparametrisation we obtain $\nabla_{\mathbf{v}}\mathbf{v} = 0$.

In [3], following [7], a formalism was presented for simplifying the system (2.1)–(2.2) on a LDRRS curve. In this case, the only degrees of freedom of the metric tensor not suppressed by the symmetries are:

$$a_{\parallel} = \sqrt{\boldsymbol{\gamma}\,(\mathbf{Z}_1, \mathbf{Z}_1)} \tag{2.14}$$

$$a_{\perp} = \sqrt{\boldsymbol{\gamma}\,(\mathbf{Z}_2, \mathbf{Z}_2)} = \sqrt{\boldsymbol{\gamma}\,(\mathbf{Z}_3, \mathbf{Z}_3)}, \tag{2.15}$$

JCAP08(2015)025

where the vectors $\mathbf{Z}_1$, $\mathbf{Z}_2$ and $\mathbf{Z}_3$ are initially equal to $\mathbf{e}_1$, $\mathbf{e}_2$ and $\mathbf{e}_3$ respectively, and their components are assumed to be constant in time in the normal coordinate basis ($\mathbf{Z}_1$, $\mathbf{Z}_2$ and $\mathbf{Z}_3$ are the coordinate basis vectors if we choose the initial coordinate system appropriately). Note that the functions $a_\parallel$ and $a_\perp$ are sufficient to reconstruct the metric tensor at any time:

$$\boldsymbol{\gamma} = a_\perp(t)^2 \left(\boldsymbol{\omega}_1 \otimes \boldsymbol{\omega}_1 + \boldsymbol{\omega}_2 \otimes \boldsymbol{\omega}_2\right) + a_\parallel(t)^2 \, \boldsymbol{\omega}_3 \otimes \boldsymbol{\omega}_3,$$

where $\boldsymbol{\omega}_i$ is the dual co-frame of $\mathbf{Z}^i$, with constant components in a normal coordinate system basis. The functions evolve according to:

$$\frac{\ddot{a}_\parallel}{a_\parallel} = \frac{2}{3} E_+, \tag{2.16}$$

$$\frac{\ddot{a}_\perp}{a_\perp} = -\frac{1}{3} E_+. \tag{2.17}$$

E_+ is the only surviving component of the electric part of the Weyl tensor, given by

$$E_+ = -\frac{3}{2} E_{ij} \, \mathbf{e}_1^i \, \mathbf{e}_1^j \tag{2.18}$$

$$E_{\mu\nu} = C_{\mu\alpha\nu\beta} \, n^\alpha \, n^\beta, \tag{2.19}$$

n^μ being the normal to the constant time slice. According to [3] its evolution is likewise governed by an ODE:

$$\dot{E}_+ = -3 \frac{\dot{a}_\perp}{a_\perp} E_+ \tag{2.20}$$

so that the evolution of the geometry on the curve is completely decoupled from its surroundings (in fact, the evolution of every single point on the curve is decoupled from all the others), and quantities that only depend on the metric tensor on the curve can be evolved using just the above system of ODEs (note that we will show in the following sections that (2.20) is missing an essential term which causes this decoupling to fail).

Such a simplified scenario is particularly suitable for use as a numerical testbed, as one can compare the results of a full three-dimensional numerical evolution to the functions $a_\parallel$, $a_\perp$ and E_+ defined above, and check to what extent the code reproduces the ODE system. We illustrate the result of this comparison in the next section.

3 Numerical Relativity solution of an S^3 black-hole lattice spacetime

3.1 Methods

We solve the full 3+1 Einstein equations for an S^3 lattice using Numerical Relativity, allowing us to compute the metric everywhere, not just on the points of high symmetry. We use the open-source Einstein Toolkit [11] and Cactus [12] framework. We compute various lattice-related analysis quantities using a Cactus code generated using Kranc [13, 14] and the xAct [15] tensor-manipulation package. Analysis of the numerical data was performed using SimulationTools for Mathematica [16].

We focus on the tesseract configuration, in which 8 identical black holes are arranged regularly on S^3. To simplify the numerical treatment, we carry out the stereographic projection, introduced in [2], from S^3 to R^3, where one of the black holes, with bare mass $m_1 = 4\mathcal{M}$

JCAP08(2015)025

is projected into the coordinate origin, another six, each with bare mass $m_{2-7} = 4\sqrt{2}\mathcal{M}$, are projected to $x^i = (\pm 2, 0, 0)\mathcal{M}$, $x^i = (0, \pm 2, 0)\mathcal{M}$, $x^i = (0, 0, \pm 2)\mathcal{M}$, and the eighth is projected out to infinity (its presence, however, is revealed by an inner trapped surface at a coordinate radius of about $20\mathcal{M}$). Here $\mathcal{M}$ is a mass parameter, and the seven m_n are the bare masses of the black holes in the Brill-Lindquist formalism (the asymmetry coming from the stereographic projection, as their physical masses are all equal to each other). The 3-metric of the $t = 0$ surface is given by:

$$\gamma_{ij} = \psi^4 \delta_{ij} \tag{3.1}$$

where δ_{ij} is the flat metric and ψ is the conformal factor, which takes the form:

$$\psi(x, y, z) = 1 + \sum_{n=1}^{7} \frac{m_n}{2r_n}\,, \tag{3.2}$$

where m_n is the bare mass of the nth black hole and r_n is the distance from it. The initial data is time-symmetric, so the extrinsic curvature is initially zero;

$$K_{ij} = 0. \tag{3.3}$$

We will study one segment of the LDRRS curve corresponding to one of the edges of the lattice lying on the diagonal between the vertices $x^i = (2/3, 2/3, 2/3)\mathcal{M}$ and $x^i = (2, 2, 2)\mathcal{M}$. The S^3 angular coordinate ϕ along this edge can be related to the Cartesian coordinates in the stereographic projection via

$$\begin{aligned} \phi &= \frac{\pi}{2} - \arccos\left(\frac{3d^2 - 4}{3d^2 + 4}\right) \\ d^2 &= \frac{4}{3}\left(\frac{1 + \sin\phi}{1 - \sin\phi}\right), \end{aligned}$$

where d is any of the coordinates x, y or z. $\phi = 0$ ($d = 2/\sqrt{3}$) corresponds to the midpoint of the edge, and most of our results will be presented using this point as an example. The vertices are located at $\phi = \pm\pi/6$.

We refer the reader to [2] for a discussion of this initial-data set, which also clarifies the role of the parameter $\mathcal{M}$ and the invariance of the spacetime under a rescaling of $\mathcal{M}$.

The spatial computational domain is $|x^i| \leq 24\sqrt{3}\mathcal{M} \approx 41.6\mathcal{M}$, and we make use of the reflection symmetry in the x, y and z directions about the coordinate planes through the origin to restrict the domain to the octant where $x \geq 0$, $y \geq 0$ and $z \geq 0$.

The Einstein equations are solved using the McLachlan [17] code with fourth order centred finite differencing for spatial derivatives and fourth order Runge-Kutta for the time integration. We integrate the Einstein equations in the BSSN formulation [18–20], a variant of the system (2.1)–(2.2). For more details, we refer the reader to [2].

In contrast to our previous work in [2], we do not use the standard binary black hole coordinate conditions (1+log slicing and gamma-driver shift), and then reslice the spacetime in postprocessing so as to use proper time as a time coordinate. Instead, we have recently found out that one can evolve this lattice directly in the normal gauge (unit lapse and zero shift), and still reach a proper time coordinate of $t \approx 110\mathcal{M}$ before the metric becomes degenerate in this coordinate system at the black holes, and further numerical evolution is not possible [21].

JCAP08(2015)025

In order to assess the effect of the numerical grid spacing on the results, we compared solutions with different overall grid spacings, labelled by the number of points, n, in one dimension in a certain coordinate distance. We report here the results for $n = 32, 40$ and 48. Since the space and time derivatives are computed with fourth order accuracy in the grid spacing $h \propto 1/n$, and this is expected to be the dominant source of error, we expect the numerical error in the solution to scale as $E = O(h^4) = O(n^{-4})$. Hence, the errors at the three resolutions should be approximately in the ratio $1 : 0.41 : 0.20$.

Due to the different length scales in the system, we use mesh refinement to concentrate the computational grid points in regions where small length and time scales need to be resolved, and avoid the prohibitive computational cost of using this same resolution everywhere. Mesh refinement is provided by the Carpet [22] code. The coarsest grid (level $L = 0$) has a grid spacing of $h_0 = \mathcal{M}/(\sqrt{3}n)$. This was chosen so that the midpoint of the edge lies on a grid point at every resolution to avoid the need to interpolate data there. Refined regions are created around each black hole (BH) and around the edge where we wish to measure quantities accurately. Several levels of refinement are used, each level having half the grid spacing and time step of its parent region, resulting in a hierarchy of nested boxes with all regions on level L completely surrounded by regions of level $L-1$. The BH at the origin, the six BHs at $r = 2$, and the edge are on levels $L = 7$, 6 and 5 respectively. The locations of the boundaries between refinement levels are found to have a significant effect on high-frequency numerical error measured on the edge. This was minimised by ensuring that the boundaries remain fixed in time and do not intersect the edge.

3.2 Results and comparison with analytic ODE

We now wish to determine whether the Numerical-Relativity (NR) spacetime satisfies the ODEs derived in [3] on the edge of the lattice. Using the NR spatial metric γ_{ij}, we compute $a_\perp$ and $a_\parallel$ as a function of time at the midpoint of the edge using (2.15) and (2.14).

In the [3] solution, the evolution of $a_\perp$ and $a_\parallel$ is determined only by E_+, and satisfies the system (2.16)–(2.17). By computing $\ddot{a}_\parallel$ and $\ddot{a}_\perp$ from the NR data, we determine E_+ from both equations. The result is shown in figure 1a, and we see that the NR evolution is consistent with (2.15) and (2.14).

According to [3], E_+ also evolves according to the ODE given by (2.20) which involves $a_\perp$ only, so that the system closes and the solution at the midpoint (as well as of any other point on the edges) decouples from its surroundings, as there are no spatial derivatives in the equation. In figure 1b, we show the NR solution for $\dot{E}_+$ and $-3\frac{\dot{a}_\perp}{a_\perp}E_+$ which should agree if the ODE derived in [3] is correct. There is a significant disagreement. We have computed the numerical error bars for figure 1, but they are too small to be visible, indicating that the disagreement is a feature of the continuum Einstein equations, and not simply due to numerical error. Figure 1c shows $a_\perp$ and $a_\parallel$ computed from NR and compared with the solution from the ODE. There is a disagreement of up to 1% which is not accounted for by the relative numerical error of $\sim 10^{-7}$. We thoroughly investigated all possible sources of error in the NR computation, and found none that could account for the discrepancy.

For future reference, we define the anomaly $\mathcal{A}$ as the unknown additional term in the equation for $\dot{E}_+$. Hence, (2.20) from [3] gets modified to:

$$\dot{E}_+ = -3\frac{\dot{a}_\perp}{a_\perp}E_+ + \mathcal{A}\,. \tag{3.4}$$

In summary, the numerical results suggest that there is a term, $\mathcal{A}$, missing in the evolution system of [3] which affects $a_\perp$ and $a_\parallel$ at the level of 1% by $t = 110\mathcal{M}$.

JCAP08(2015)025

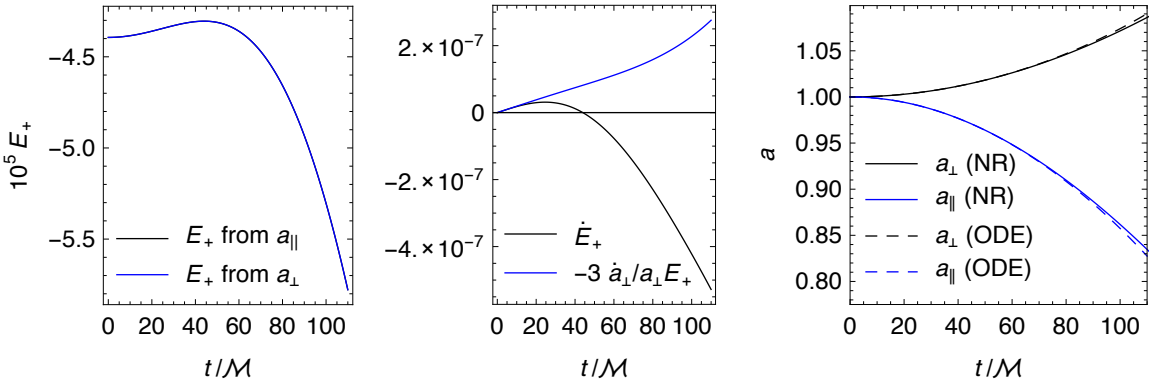

(a) Consistency of E_+ computed from the NR $a_\perp$ and $a_\parallel$.

(b) Violation of the ODE $\dot{E}_+ = -3\frac{\dot{a}_\perp}{a_\perp}E_+$ by the NR solution.

(c) $a_\perp$ and $a_\parallel$ differ by up to 1% between the NR and ODE solutions. This is much larger than the relative numerical error of 10^{-7}.

Figure 1. Comparison between Numerical Relativity and ODE.

4 The evolution equations on a LDRRS curve

We now turn our attention again to the ODE system formed by (2.16), (2.17) and (2.20), and in particular attempt to show that it is the reduction of the system (2.1)–(2.2) on a LDRRS curve.

Equations (2.1)–(2.4) for γ_{ij} and K_{ij} are not closed at a single point because of the presence of the spatial derivatives of γ_{ij} in the 3-dimensional Ricci tensor R_{ij}. We will try to close the system by extending it to include R_{ij} as a new evolution variable, for which we require the time derivative of R_{ij}. Recall that the time derivative of the 3-dimensional Ricci tensor takes the form

$$\dot{R}_{ij} = \frac{1}{2}\left(\dot{\gamma}^k{}_{i;jk} + \dot{\gamma}^k{}_{j;ik} - \dot{\gamma}^k{}_{k;ij} - \dot{\gamma}_{ij;k}{}^k\right),$$

where the indices have been raised by the inverse metric γ^{ij}, i.e. $\dot{\gamma}^k{}_i = \dot{\gamma}_{ji}\,\gamma^{jk}$. We substitute (2.1) to obtain

$$\dot{R}_{ij} = K^k{}_{k;ij} + K_{ij;k}{}^k - K^k{}_{i;jk} - K^k{}_{j;ik}.$$

We would like to get rid of the second derivatives in the equation above. This obviously requires permuting the indices in the expressions above. Swapping the first or the second pair of the indices is straightforward, but exchanging two indices between the two pairs is less obvious. We introduce the following notation for the antisymmetrisation in the indices 2 and 3:

$$U_{ijkl} = K_{ij;kl} - K_{ik;jl}. \tag{4.1}$$

After a tedious exercise in index manipulation we arrive at the following expression for the time derivative of the Ricci tensor

$$\dot{R}_{ij} = R^k{}_{p(i\|k\|}\,K^p{}_{j)} - R^p{}_{(ij)k}\,K^k{}_p + U_{(ij)k}{}^k, \tag{4.2}$$

JCAP08(2015)025

where $\|\cdot\|$ excludes an index from symmetrisation and $R^{i}{}_{jkl}$ denotes the Riemann tensor of γ_{ij}. In three dimensions R_{ijkl} can be expressed entirely via the Ricci tensor and the Ricci scalar [23]:

$$R_{ijkl} = R_{jl}\,\gamma_{ik} - R_{il}\,\gamma_{jk} - R_{jk}\,\gamma_{il} + R_{ik}\,\gamma_{jl} + \frac{1}{2}R\,(\gamma_{il}\,\gamma_{jk} - \gamma_{jl}\,\gamma_{ik})\,.$$

If we substitute the relation above into (4.2) we obtain

$$\begin{aligned}\dot{R}_{ij} = &-\frac{3}{2}\left(R_i{}^k\,K_{kj} + R_j{}^k\,K_{ki}\right) + K_{kl}\,R^{kl}\gamma_{ij} \\ &+\frac{1}{2}R\,K_{ij} + K\,R_{ij} - \frac{1}{2}R\,K\,\gamma_{ij} + U_{(ij)k}{}^{k},\end{aligned} \tag{4.3}$$

i.e. the time derivative of the Ricci tensor expressed directly via γ_{ij}, K_{ij} and R_{ij} and a single additional term $U_{(ij)k}{}^{k}$. The last term, i.e. the symmetrized contraction of U_{ijkl}, is now the only one involving the spatial derivatives of K_{ij} and γ_{ij} and thus not expressible directly via γ_{ij}, K_{ij} and R_{ij}. We will introduce a new notation for the contraction:

$$U_{ij} = U_{ijk}{}^{k}. \tag{4.4}$$

4.1 Properties of U_{ijkl} and relation to the magnetic part of the Weyl tensor

Before we proceed with the derivation of the reduced Einstein equations, we will discuss some of the properties of U_{ijkl} and elucidate its relation to the magnetic part of the Weyl tensor. Recall that the Weyl tensor $C_{\mu\nu\alpha\beta}$ in a 3+1 decomposition may be represented by its electric and magnetic parts defined via (2.19) and

$$B_{\mu\nu} = -\frac{1}{2}C_{\mu\alpha\kappa\lambda}\,\eta^{\kappa\lambda}{}_{\nu\beta}n^{\alpha}\,n^{\beta} \tag{4.5}$$

respectively, n^{μ} being again the normal to the constant time slice, and $\eta^{\kappa\lambda}{}_{\nu\beta}$ denoting the totally antisymmetric volume form [24, 25]. Both tensors vanish in the normal direction and can be considered 3-dimensional, spatial objects. The magnetic part of the Weyl tensor in the ADM variables can be related to the tensorial curl of the extrinsic curvature:

$$B_{ij} = \eta_j{}^{kl}K_{ik;l}\,. \tag{4.6}$$

We can easily prove that it is traceless and symmetric: first, we note that

$$B^{i}{}_{i} = \eta^{ikl}K_{ik;l} = 0$$

because K_{ik} is symmetric with respect to the exchange of the indices. The contraction of B_{ij} with another volume form is equal to zero as well:

$$B_{ij}\,\eta^{ijp} = -\left(\gamma^{ki}\,\gamma^{lp} - \gamma^{kp}\,\gamma^{li}\right)K_{ik;l} = K^{pl}{}_{;l} - K^{;p} = 0,$$

where the last expression vanishes because of the vector constraint equation (2.4). Note that in three dimensions this implies the vanishing of the whole antisymmetric part of B_{ij}, so $B_{ij} = B_{(ij)}$.

The covariant derivative of B_{ij} on the other hand can be related to $\mathbf{U}$ via

$$U_{ijkl} = B_{ip;l}\,\eta^{p}{}_{jk}.$$

JCAP08(2015)025

The equation above, contracted with respect to the two last indices, yields

$$U_{ij} = -\eta_j{}^{pl}\, B_{ip;l}, \tag{4.7}$$

which has exactly the same structure as (4.6), i.e. U_{ij} is proportional to the curl of B_{ij}. Now, repeating the reasoning we have used for B_{ij} above we may prove that the trace of (4.7) vanishes because of the symmetry of B_{ij}.[1]

$$U^i{}_i = 0. \tag{4.8}$$

4.2 The reduced evolution equations

Consider the tangent space at a point along a LDRRS curve λ. We rewrite (2.1)–(2.2) and (4.3) assuming conditions (2.11)–(2.13) to hold and parametrizing the metric according to (2.14)–(2.15). We first note that the antisymmetric part of $U_{ijk}{}^k$ must vanish because of (2.13). Since it is also traceless it must be proportional to U_{11} (see (2.12)). We obtain (2.16)–(2.17), where E_+ is the non-vanishing part of the electric Weyl tensor, but (2.20) now takes the form of

$$\dot{E}_+ = -3\tfrac{\dot{a}_\perp}{a_\perp} E_+ - \tfrac{3}{2} U_{11}, \tag{4.9}$$

with $U_{11} = U_{ij}\, \mathbf{e}_1^i\, \mathbf{e}_1^j$ (notice that numeric indices always indicate frame components). In [3], the authors assume that this term vanishes due to the rotation and reflection invariance.[2] We will show that this is not the case in general. As a result, we will identify this term with the anomaly $\mathcal{A}$ found numerically in section 3.2;

$$\mathcal{A} = -\frac{3}{2} U_{11}\,. \tag{4.10}$$

First let us consider the magnetic part of the Weyl tensor. Since B_{ij} is composed of rotation-invariant η_{ijk} and $K_{ij;k}$ it is rotation-invariant itself. Being additionally traceless and symmetric it must be proportional to B_{11} due to (2.12). From (4.6) we obtain

$$B_{11} = K_{12;3} - K_{13;2} = 2K_{i[2;3]}\, \mathbf{e}_1^i\,. \tag{4.11}$$

Since $\mathbf{e}_1$ is both rotation- and reflection-invariant, the last expression is the $(2,3)$ component of a rotation- and reflection-invariant rank 2 antisymmetric tensor, so it must vanish at λ because of (2.13).

Now, since U_{ij} is also traceless and is given by a very similar expression (4.7) to B_{ij}, it would be tempting to repeat the argument above and conclude that U_{11}, together with the whole symmetric part of U_{ij}, vanishes too. This would however be incorrect due to the following: unlike K_{ij} appearing in (4.6), B_{ij} in (4.7) is *not* reflection-invariant. Note that since its definition (4.6) involves the volume form η_{ijk} it changes its sign under reflections (2.8)–(2.10). Although U_{11} can be put in a similar form to (4.11):

$$U_{11} = -2B_{i[2;3]}\, \mathbf{e}_1^i$$

[1] Note however that U_{ij} does not have to be symmetric in general, unlike B_{ij}.

[2] It corresponds to the term proportional to $\epsilon^{\gamma\delta(\alpha}\, \mathbf{e}_\gamma \left(H^{\beta)}{}_\delta\right)$ in equation (2.15) in the aforementioned paper. If it does not vanish then it appears later in the evolution equation (4.11).

JCAP08(2015)025

we cannot now apply (2.13) because the antisymmetric 2-tensor in question $B_{i[k;l]}\,\mathbf{e}_1^i$ is *not* reflection-invariant. The symmetry assumptions put no restrictions on the value of U_{11} and there no reason whatsoever to assume that U_{11} vanishes identically along a LDRRS curve.

We can give a simple and instructive analogy from the theory of electromagnetism and Maxwell's equations. Consider a static configuration of electric and magnetic fields in a flat space exhibiting a similar rotation and reflection invariance with respect to a chosen axis. If the vector potential $\vec{A}$ is invariant then its curl needs to vanish at the symmetry axis and thus the magnetic field $\vec{B} = \operatorname{curl} \vec{A} = 0$ along the axis due to the reflection symmetry, just like in the case of the magnetic Weyl tensor. But the curl of $\vec{B}$ *does not* need to vanish at the axis. Indeed, it is easy to create a configuration of the electromagnetic field in which there is a non-vanishing current flowing along the axis and thus $\vec{j} = \operatorname{curl} \vec{B} \neq 0$. This is due to the fact that $\vec{B}$, as a curl of a vector, is a pseudovector field, while $\vec{j}$, which is a *curl of a curl* of a vector is again a regular vector field. The former must vanish because of the reflection symmetry, but the latter not.

4.3 U_{11} and its time derivatives for the 8-black-hole initial data

The initial data described in section 3.1 is time-symmetric, so the solution in normal coordinates satisfies $\gamma_{ij}(t) = \gamma_{ij}(-t)$. It follows that the odd time derivatives of the metric $\frac{\partial^{2N+1}}{\partial t^{2N+1}}\gamma_{ij}$ and of the Christoffel symbols $\frac{\partial^{2N+1}}{\partial t^{2N+1}}\Gamma^i{}_{jk}$, $N = 0, 1, 2\ldots$, vanish at $t = 0$ identically. So does the extrinsic curvature together with its even time derivatives $\frac{\partial^{2N}}{\partial t^{2N}}K_{ij}$. From (4.1) and (4.4) we see that the same must hold for U_{ij}, i.e.

$$\frac{\partial^{2N}}{\partial t^{2N}}U_{ij} = 0 \qquad \text{at} \quad t = 0$$

and in particular U_{ij} and $\ddot{U}_{ij}$ vanish initially. Direct computation reveals that for the initial data (3.3) and (3.1) the first derivative $\dot{U}_{ij} = 0$ along a LDRRS curve vanishes as well. The first non-vanishing time derivative turns out to be the third one. We have evaluated it as a combination of the partial derivatives of the conformal factor ψ. Since the expression involves up to 4th covariant derivatives of the Ricci tensor of γ_{ij}, the tensor manipulations and algebraic reduction were performed using Mathematica. The final result, considered along the LDRRS curve and after simplifications due to the symmetry, reads

$$\begin{aligned}
U_{11}^{(3)}\Big|_{t=0} = 2\psi^{-18}\Big(&-\Big(\psi^{(0,0,6)} + 3\psi^{(0,2,4)} + 3\psi^{(0,4,2)} + \psi^{(0,6,0)} \\
&+2\left(\psi^{(2,0,4)} + 2\psi^{(2,2,2)} + \psi^{(2,4,0)}\right) - \psi^{(6,0,0)}\Big)\psi^5 \\
&+\Big(-8(\psi^{(3,0,0)})^2 + \psi^{(2,0,0)}\left(35\psi^{(4,0,0)} - 29\left(\psi^{(0,0,4)} + 2\psi^{(0,2,2)} + \psi^{(0,4,0)}\right)\right) \\
&+2\Big(24(\psi^{(0,0,3)})^2 + 44\psi^{(0,2,1)}\psi^{(0,0,3)} + 28(\psi^{(0,1,2)})^2 + 28(\psi^{(0,2,1)})^2 + 24(\psi^{(0,3,0)})^2 \\
&+44\psi^{(0,1,2)}\psi^{(0,3,0)} + 6\psi^{(0,1,1)}\left(\psi^{(0,1,3)} + \psi^{(0,3,1)}\right) + 7\psi^{(1,0,1)}\left(\psi^{(1,0,3)} + \psi^{(1,2,1)}\right) \\
&+7\psi^{(1,1,0)}\left(\psi^{(1,1,2)} + \psi^{(1,3,0)}\right) + 2\psi^{(1,0,0)}\left(\psi^{(1,0,4)} + 2\psi^{(1,2,2)} + \psi^{(1,4,0)} - \psi^{(5,0,0)}\right)\Big)\Big)\psi^4 \\
&-2\Big(18(\psi^{(2,0,0)})^3 - 24\psi^{(1,0,0)}\psi^{(3,0,0)}\psi^{(2,0,0)} + 2\psi^{(0,0,4)}(\psi^{(0,1,0)})^2 + 11(\psi^{(0,0,1)})^2\psi^{(0,0,4)} \\
&+18\psi^{(0,0,1)}\psi^{(0,1,0)}\psi^{(0,1,3)} + 13(\psi^{(0,0,1)})^2\psi^{(0,2,2)} + 13(\psi^{(0,1,0)})^2\psi^{(0,2,2)}
\end{aligned}$$

JCAP08(2015)025

$$
\begin{aligned}
&+18\psi^{(0,0,1)}\psi^{(0,1,0)}\psi^{(0,3,1)} + 2(\psi^{(0,0,1)})^2\psi^{(0,4,0)} + 11(\psi^{(0,1,0)})^2\psi^{(0,4,0)} \\
&+7\psi^{(1,0,0)}\left(7\left(\psi^{(0,0,3)} + \psi^{(0,2,1)}\right)\psi^{(1,0,1)} + 7\left(\psi^{(0,1,2)} + \psi^{(0,3,0)}\right)\psi^{(1,1,0)}\right. \\
&\left.+3\psi^{(0,0,1)}\left(\psi^{(1,0,3)} + \psi^{(1,2,1)}\right) + 3\psi^{(0,1,0)}\left(\psi^{(1,1,2)} + \psi^{(1,3,0)}\right)\right) - 8(\psi^{(0,0,1)})^2\psi^{(4,0,0)} \\
&-8(\psi^{(0,1,0)})^2\psi^{(4,0,0)} + (\psi^{(1,0,0)})^2\left(26\psi^{(4,0,0)} - 20\left(\psi^{(0,0,4)} + 2\psi^{(0,2,2)} + \psi^{(0,4,0)}\right)\right)\Big)\psi^3 \\
&-6\left(3\left((\psi^{(0,0,1)})^2 + (\psi^{(0,1,0)})^2\right)(\psi^{(2,0,0)})^2 - \psi^{(1,0,0)}\left(49\left(\psi^{(0,0,1)}\left(\psi^{(0,0,3)} + \psi^{(0,2,1)}\right)\right.\right.\right. \\
&\left.\left.\left.+\psi^{(0,1,0)}\left(\psi^{(0,1,2)} + \psi^{(0,3,0)}\right)\right)\psi^{(1,0,0)} - 8\left((\psi^{(0,0,1)})^2 + (\psi^{(0,1,0)})^2\right)\psi^{(3,0,0)}\right)\right)\psi^2 \\
&+288\left((\psi^{(0,0,1)})^2 + (\psi^{(0,1,0)})^2\right)(\psi^{(1,0,0)})^2\psi^{(2,0,0)}\psi \\
&-288\left((\psi^{(0,0,1)})^2 + (\psi^{(0,1,0)})^2\right)(\psi^{(1,0,0)})^4\Big)\,,
\end{aligned}
\tag{4.12}
$$

where we have assumed above that the first coordinate x^1 is aligned along the curve and x^2, x^3 are transversal. We have introduced here a short hand notation for the partial derivatives in the form of $\psi^{(p,q,r)} = \frac{\partial^p}{\partial(x^1)^p}\frac{\partial^q}{\partial(x^2)^q}\frac{\partial^r}{\partial(x^3)^r}\psi$. Substituting the conformal factor ψ from equation (3.2), we obtain that the numerical value of $U_{11}^{(3)}(0)$ at the midpoint of the edge is 4.3×10^{-12}.

4.4 Effect of U_{11} on the metric

The addition of the term $-3/2U_{11}$ to the ODE clearly affects the evolution of $a_\parallel$ and $a_\perp$. We can estimate the effect by making a Taylor expansion of $a_\parallel(t)$ and $a_\perp(t)$ about $t = 0$ and using the evolution equations (2.17), (2.16) and (4.9) to evaluate the Taylor coefficients at $t = 0$. We find that the effect of U_{11} appears first in the $O(t^6)$ term. Using an overbar to represent the solution using the original ODE (2.20), i.e. without the U_{11} term, we find

$$
\Delta a_\parallel = a_\parallel - \bar{a}_\parallel \;= -\frac{a_\parallel(0)}{720}U_{11}^{(3)}(0)t^6 + O(t^8) \tag{4.13}
$$

$$
\Delta a_\perp = a_\perp - \bar{a}_\perp = \frac{a_\perp(0)}{1440}U_{11}^{(3)}(0)t^6 + O(t^8)\,, \tag{4.14}
$$

where we have used the fact that $a_\perp$, $a_\parallel$ and E_+ have the same value at $t = 0$ independent of the appearance of U_{11} in the ODE.

At the midpoint of the edge, at $t = 110\mathcal{M}$, we find a relative error $\Delta a_\parallel/a_\parallel$ of about 1% compatible with the NR results in figure 1c, and a relative error of 100% by $t = 235\mathcal{M}$. We conclude that the leading order contribution to U_{11} leads to a complete breakdown of the original ODE solution by this time, though we cannot determine whether higher order corrections are important here.

5 Numerical Relativity calculation of U_{11}

5.1 Consistency between NR and new analytical results

In the previous section, we identified a term, $-3/2U_{11}$, in the evolution equation for $\dot{E}_+$ which was assumed in [3] to vanish, but for which we find a nonvanishing third time derivative. We

JCAP08(2015)025

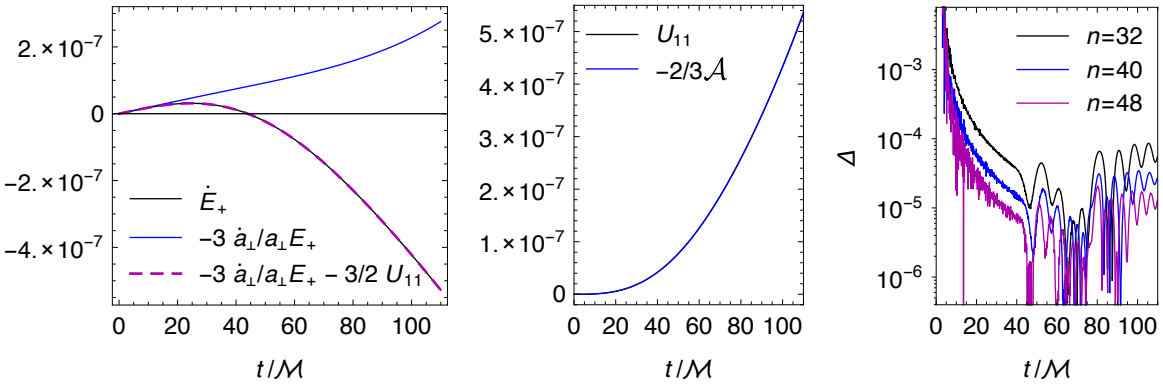

(a) Comparison of $\dot{E}_+$ with the original and new right-hand sides.

(b) U_{11} and $-2/3\mathcal{A}$ computed from NR.

(c) $\Delta \equiv 1 - (-2/3\mathcal{A})/U_{11}$ computed from NR at several resolutions.

Figure 2. NR solution demonstrating consistency with the new analytic results.

now aim to verify that the NR solution satisfies the new evolution equation (4.9), and that the numerically-non-zero anomaly $\mathcal{A}$ is indeed related to U_{11} by (4.10). U_{11} is computed in NR from covariant derivatives of the extrinsic curvature,

$$U_{11} = (K_{ij;k}{}^{k} - K_{ik;j}{}^{k})\, \mathbf{e}_1^i\, \mathbf{e}_1^j\,, \tag{5.1}$$

whereas $\mathcal{A}$ is defined via (3.4).

Figure 2a shows a comparison between $\dot{E}_+$ and the r.h.s. of the original and new evolution equations. We see that the addition of the term $-3/2U_{11}$ is necessary for agreement. In figure 2b, we see that U_{11} and $-2/3\mathcal{A}$ are found to be indistinguishable, and figure 2c shows that their relative difference, $\Delta \equiv 1 - (-2/3\mathcal{A})/U_{11}$, converges to zero as the numerical resolution n is increased. The convergence is 4th order, as expected from the finite differencing order of the code. Δ exhibits high-frequency noise for $t < 40\mathcal{M}$ which we attribute to error coming from the finite precision with which floating point numbers are represented in the code.[3] We have partially filtered the high frequency noise from the data in figure 2c to make the convergence more apparent. For $t > 40\mathcal{M}$, there are lower-frequency oscillations in the error which we attribute to numerical reflections from mesh refinement boundaries.

For $t > 20\mathcal{M}$, at the highest resolution, we see that $|\Delta| < 3 \times 10^{-5}$. Hence

$$-\frac{2}{3}\mathcal{A} = 1.00000(3)\, U_{11} \tag{5.2}$$

in agreement with the analytic derivation in section 4.2. For $t < 20\mathcal{M}$, the ratio is still consistent with $-2/3$, but the relative error is larger since U_{11} itself is small.

We therefore see that the anomaly originally measured in the comparison of the 3+1 Numerical Relativity results and the ODE system presented in [3] was due to the term U_{11} derived in the previous section, but taken to vanish in the original derivation.

[3] $\mathcal{A}$ depends on the third time derivative of $a_\perp$, and an initial relative roundoff error of $\epsilon \sim 10^{-15}$ with frequency $\omega \sim \pi/\Delta t \sim 80$, for Δt the time spacing of output data points, will be amplified by a factor of $a_\perp/\dddot{a}_\perp\omega^3$ when taking a third derivative, which leads to a relative error in $\ddot{a}_\perp$ comparable with that observed for the measured values of $a_\perp \sim 10^2$ and $\ddot{a}_\perp \sim 10^{-7}$.

JCAP08(2015)025

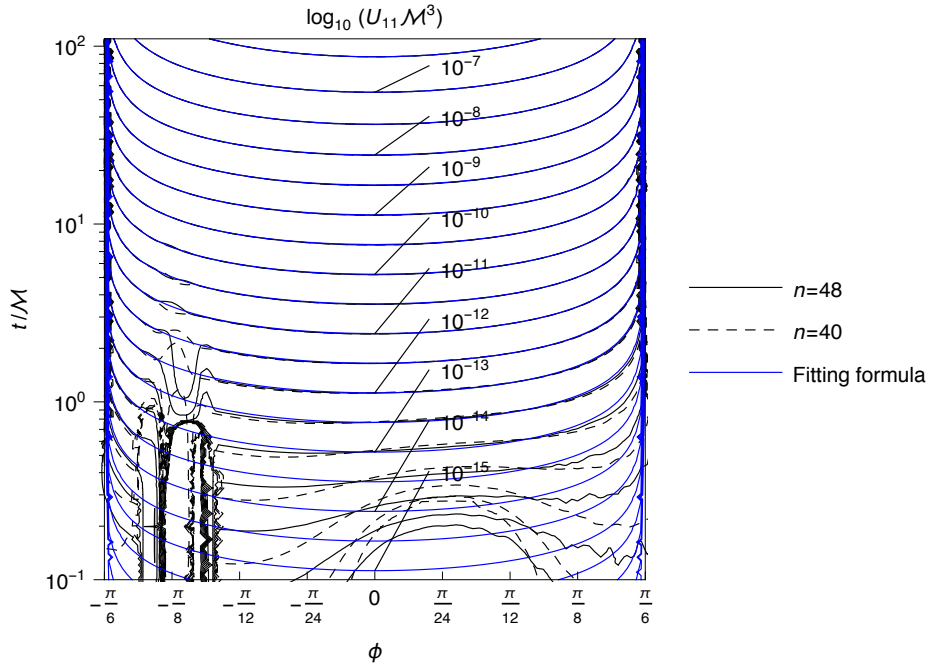

Figure 3. Contours of $\log_{10} U_{11}$ computed using NR at two different resolutions (solid and dashed black contours) and from a simple polynomial formula fitted to the NR data (blue contours) as a function of t (time) and ϕ (coordinate along the edge). The fit is performed in the region $1\mathcal{M} \leq t \leq 110\mathcal{M}$.

5.2 Computation of U_{11} and fitting formula

We now present the NR computation of U_{11} on the edge, and give a simple fitting formula for it that could be used along with (4.9) to solve the system via an ODE.

Figure 3 is a contour plot of $\log_{10}(U_{11}\mathcal{M}^3)$ as a function of t and ϕ, the proper time and the S^3 angular coordinate along the edge, respectively. The black solid and dashed lines represent contours of U_{11} computed at resolutions $n = 48$ and $n = 40$ respectively. For $t \geq 10\mathcal{M}$ the two resolutions are indistinguishable, indicating that the numerical error is small in comparison with U_{11}. For $t < 10\mathcal{M}$, there are regions, notably around $\phi \sim -\pi/8$, where the numerical error dominates over U_{11}, which at these early times is $O(10^{-15})$. The NR data satisfies $U_{11}(0, \phi) = U_{11}(t, \pm\pi/6) = 0$ on the initial slice and the vertices as expected, since $U_{11} = 0$ there by symmetry. Note that the NR computation was performed in Cartesian coordinates (t, x, y, z) and has been transformed to $\left(t, \phi = \frac{\pi}{2} - \cos^{-1}\left(\frac{3x^2-4}{3x^2+4}\right)\right)$ for plotting. While the spacetime is symmetric about $\phi = 0$ in (t, ϕ), this is not the case in (t, x, y, z), hence the continuum solution is expected to show this symmetry in ϕ, but the numerical error is not. This is reflected in figure 3.

Since U_{11} is only available numerically, and appears to have a simple form in the regions in which it is well resolved, we provide a simple formula based on low-order polynomials in t and ϕ obtained via a least-squares fit to the NR data in the region $1\mathcal{M} \leq t \leq 110\mathcal{M}$, $-\pi/6 \leq \phi \leq \pi/6$, corresponding to the edge of the lattice. The fitting formula is

$$U_{11} = \sum_{p,q} c_{pq} (t/\mathcal{M})^p \phi^q \mathcal{M}^{-3} \qquad p = 3, 5, 7 \quad q = 0, 2, 4, 6 \tag{5.3}$$

with the coefficients c_{pq} of $(t/\mathcal{M})^p$ and ϕ^q given in table 1. The error estimate in the last

JCAP08(2015)025

	1	ϕ^2	ϕ^4	ϕ^6
$(t/\mathcal{M})^3$	$7{\cdot}040(1) \times 10^{-13}$	$-3{\cdot}558(6) \times 10^{-12}$	$4{\cdot}23(4) \times 10^{-12}$	$-2{\cdot}30(7) \times 10^{-12}$
$(t/\mathcal{M})^5$	$-3{\cdot}810(2) \times 10^{-17}$	$2{\cdot}361(9) \times 10^{-16}$	$-4{\cdot}37(6) \times 10^{-16}$	$3{\cdot}1(1) \times 10^{-16}$
$(t/\mathcal{M})^7$	$1{\cdot}0965(9) \times 10^{-21}$	$-6{\cdot}85(3) \times 10^{-21}$	$1{\cdot}30(2) \times 10^{-20}$	$-9{\cdot}8(3) \times 10^{-21}$

Table 1. Coefficients of $(t/\mathcal{M})^p$ and ϕ^q in the fitting formula for U_{11} determined from NR.

digit in parentheses is an indication of numerical truncation error. The contours of the fitting formula are shown in blue in figure 3.

The region $1\mathcal{M} \leq t \leq 10\mathcal{M}$ contains localised regions of high relative numerical error, but the small number of degrees of freedom in the fitting formula means that the fit is insensitive to these localised regions. The region $t \leq 1\mathcal{M}$, in which the NR error dominates, is outside the fit region, and hence the fitting formula is an extrapolation in this region. For $t > 10\mathcal{M}, |\phi| < \pi/8$, i.e. the regions where U_{11} is not close to zero, this fitting function approximates the NR result to within $\pm 1\%$. In the regions $t < 10\mathcal{M}$ and $|\phi| > \pi/8$, the absolute agreement is within $10^{-12}\mathcal{M}^{-3}$.

For $t \geq 10\mathcal{M}$, the NR and fitting-formula curves are visually indistinguishable.

5.3 Computation of $U_{11}^{(3)}$

We now wish to compute the third time derivative of U_{11} at $\phi = 0$ from the NR data and compare with the analytic result obtained in (4.12). We cannot directly finite-difference the NR data near $t = 0$ because, as can be seen in figure 3, it is contaminated by numerical error. Instead, we compute the derivative by analytically differentiating the fitting formula. The fitting effectively averages out the very small numerical errors near $t = 0$ and uses information from $t > 0$, where the errors are less significant, to obtain information about the derivative at $t = 0$.

The fitting formula (5.3) contains only a finite number of terms, so the coefficients cannot be directly identified with the coefficients in a Taylor series, and hence with the derivatives of U_{11}. However, as the number of terms in the fitting formula is increased, we expect the coefficients to approach the Taylor coefficients. We find that as both $p_{\max}$ and $q_{\max}$ are increased, c_{30} appears to converge exponentially towards a limiting value. Taking this to be the Taylor coefficient, we obtain an NR estimate for $U_{11}^{(3)}$ which can be directly compared with the analytic value obtained from (4.12):

$$\left.\frac{\partial^3 U_{11}}{\partial t^3}\right|_{t=0,\phi=0} = \begin{cases} 4.3015(4) \times 10^{-12}\mathcal{M}^{-6} & \text{Numerical} \\ 4.30113 \times 10^{-12}\mathcal{M}^{-6} & \text{Analytic}\,. \end{cases} \tag{5.4}$$

The NR error estimate in parentheses includes the effect of both numerical truncation error and of fitting using a finite number of terms, and we see that the NR derivative matches the analytical calculation within NR errors. We therefore have a high degree of confidence that the numerical solution and our understanding of the analytical system are correct.

5.4 Effect of U_{11}

In figure 4, we show the relative difference between $a_\parallel$ computed from NR and from the original ODE, and compare it with the leading order analytic contribution computed in section 4.4 from the Taylor series. We see that the relative difference is dominated by the

JCAP08(2015)025

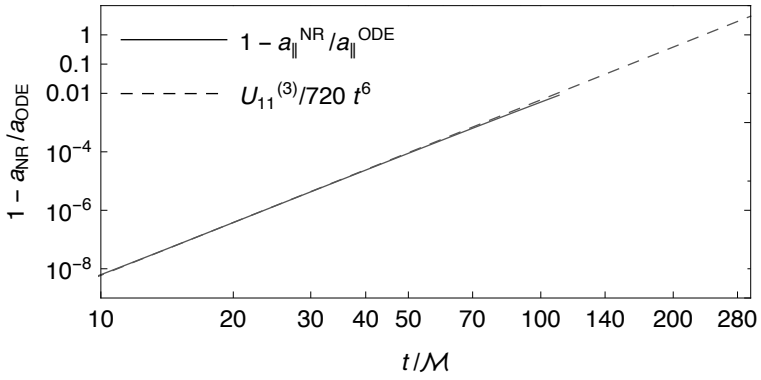

Figure 4. Comparison between the difference between the NR and ODE solutions for $a_{\parallel}$, and the leading order contribution computed from a Taylor expansion.

leading order term for as long as the NR computation lasts. We do not know whether this will continue past $t = 110\mathcal{M}$.

6 Conclusions

We have solved the full Einstein equations for an S^3 8-black-hole lattice spacetime using Numerical-Relativity and found that the solution along certain LDRRS curves does not agree with the ODEs previously derived for this system.

We therefore analysed the behaviour of LDRRS curves in vacuum spacetimes, and in particular showed that the evolution of certain symmetric subsets does not decouple from the surrounding spacetime, following a system of pure ODEs, as had been previously claimed. Instead, the variables $a_{\parallel}$, $a_{\perp}$ and E_{+}, which capture all the metric and extrinsic-curvature degrees of freedom not suppressed by the symmetries, follow a system of ODEs with a source term U_{11}, which itself depends on the spatial derivatives of the extrinsic curvature and can only, to our knowledge, be computed via Numerical Relativity.

We have then computed this term using Numerical Relativity, both as an anomaly in the original ODE system, and via its expression in terms of the derivatives of K_{ij}. These agree to within the relative numerical error of 3×10^{-5}, strengthening our confidence in both the analytical study performed in sections 2 and 4 and the numerical infrastructure used in sections 3 and 5, as well as in [2].

Note that it is still possible to use the ODE system presented in [3], as long as one knows the source term independently. To this end, we provide a polynomial function, fitted from the NR data, in both proper time t and edge coordinate ϕ, which can be used up until $t \sim 110\mathcal{M}$. We have also computed the third time derivative of U_{11} on the midpoint of the edge at $t = 0$ (which is the lowest non-zero time derivative of U_{11} initially), and compared it with an analytical derivation of the same quantity in the ADM formalism. These also agree within the relative numerical error of 10^{-4}.

We conclude by remarking that the evolution of the edges of S^3 black-hole lattices is not symmetric enough for a reduced-dimension calculation,[4] and can, to our knowledge, only be performed via Numerical Relativity. In particular, the solution to the ODE system presented

[4]Note that the vertices, on the other hand, possess enough symmetries for a full decoupling from the neighbouring points, leading to the solution $E_{+} = 0$ and the 3-metric being constant.

JCAP08(2015)025

in [3] can be treated as an approximation, valid at early times, which may or may not be close to the true solution at late times. We have measured the error associated with such an approximation by direct comparison with a 3+1 integration of the Einstein equations, and find it to grow to $\sim 1\%$ in the components of the spatial metric for $t \lesssim 110\mathcal{M}$. We have shown analytically that the leading order effect of the U_{11} term is $O(t^6)$ in the metric, and this is observed to a very good approximation in the NR results for $t < 110\mathcal{M}$. The duration of the NR computations presented here is limited by the use of the normal gauge, and at the present time, we have no way of assessing the error resulting from neglecting the U_{11} term at late times far from the time-symmetric hypersurface. We observe that if the t^6 growth were to continue, the metric would have 100% error by $t \sim 235\mathcal{M}$. At late times, the results obtained from the system derived in [3] may well be qualitatively different to those that would be obtained by an evolution using the full, corrected, system.

Acknowledgments

MK and EB would like to thank the Max Planck Institute for Gravitational Physics (Albert Einstein Institute) in Potsdam for hospitality. The work was supported by the project *"The role of small-scale inhomogeneities in general relativity and cosmology"* (HOMING PLUS/2012-5/4), realized within the Homing Plus programme of Foundation for Polish Science, co-financed by the European Union from the Regional Development Fund, and by the project "*Digitizing the universe: precision modelling for precision cosmology*", funded by the Italian Ministry of Education, University and Research (MIUR). The Numerical Relativity computations were performed on the Datura cluster at the AEI. Code for solving the ODEs was written in collaboration with Mikołaj Bińkowski. We thank Timothy Clifton for reading a draft of this manuscript and pointing out several typographical errors. Any remaining mistakes and omissions remain the responsibility of the authors.

References

[1] T. Clifton, K. Rosquist and R. Tavakol, *An Exact quantification of backreaction in relativistic cosmology*, *Phys. Rev.* **D 86** (2012) 043506 [arXiv:1203.6478] [INSPIRE].

[2] E. Bentivegna and M. Korzyński, *Evolution of a periodic eight-black-hole lattice in numerical relativity*, *Class. Quant. Grav.* **29** (2012) 165007 [arXiv:1204.3568] [INSPIRE].

[3] T. Clifton, D. Gregoris, K. Rosquist and R. Tavakol, *Exact Evolution of Discrete Relativistic Cosmological Models*, *JCAP* **11** (2013) 010 [arXiv:1309.2876] [INSPIRE].

[4] T. Clifton, D. Gregoris and K. Rosquist, *Piecewise Silence in Discrete Cosmological Models*, *Class. Quant. Grav.* **31** (2014) 105012 [arXiv:1402.3201] [INSPIRE].

[5] T. Clifton, *The Method of Images in Cosmology*, *Class. Quant. Grav.* **31** (2014) 175010 [arXiv:1405.3197] [INSPIRE].

[6] R.G. Liu and R.M. Williams, *Regge calculus models of closed lattice universes*, arXiv:1502.03000 [INSPIRE].

[7] H. van Elst and C. Uggla, *General relativistic* $(1+3)$ *orthonormal frame approach revisited*, *Class. Quant. Grav.* **14** (1997) 2673 [gr-qc/9603026] [INSPIRE].

[8] R. Arnowitt, S. Deser and C. W. Misner, *The dynamics of general relativity*, in *Gravitation: An introduction to current research*, L. Witten ed., chapter 7, Wiley, New York U.S.A. (1962), pp. 227–265 [*Gen. Rel. Grav.* **40** (2008) 1997] [gr-qc/0405109] [INSPIRE].

JCAP08(2015)025

[9] J.W. York Jr., *Kinematics and dynamics of general relativity*, in *Sources of Gravitational Radiation*, L.L. Smarr ed., Cambridge University Press (1979), pp. 83–126.

[10] P. Anninos, *Computational cosmology: From the early universe to the large scale structure*, *Living Rev. Rel.* **4** (2001) 2 [gr-qc/0108083] [INSPIRE].

[11] F. Löffler et al., *The Einstein Toolkit: A Community Computational Infrastructure for Relativistic Astrophysics*, *Class. Quant. Grav.* **29** (2012) 115001 [arXiv:1111.3344] [INSPIRE].

[12] *Cactus computational toolkit*, http://www.cactuscode.org.

[13] S. Husa, I. Hinder and C. Lechner, *Kranc: A Mathematica application to generate numerical codes for tensorial evolution equations*, *Comput. Phys. Commun.* **174** (2006) 983 [gr-qc/0404023] [INSPIRE].

[14] S. Husa, I. Hinder, C. Lechner, E. Schnetter and B. Wardell, *Kranc: Automatic numerical code generation*, http://kranccode.org.

[15] J.M. Martín-García, *xPerm: fast index canonicalization for tensor computer algebra*, *Comput. Phys. Commun.* **179** (2008) 597 [arXiv:0803.0862] [http://www.xact.es].

[16] I. Hinder and B. Wardell, *SimulationTools for Mathematica*, http://simulationtools.org.

[17] J.D. Brown, P. Diener, O. Sarbach, E. Schnetter and M. Tiglio, *Turduckening black holes: An Analytical and computational study*, *Phys. Rev.* **D 79** (2009) 044023 [arXiv:0809.3533] [INSPIRE].

[18] T. Nakamura, K. Oohara and Y. Kojima, *General Relativistic Collapse to Black Holes and Gravitational Waves from Black Holes*, *Prog. Theor. Phys. Suppl.* **90** (1987) 1 [INSPIRE].

[19] M. Shibata and T. Nakamura, *Evolution of three-dimensional gravitational waves: Harmonic slicing case*, *Phys. Rev.* **D 52** (1995) 5428 [INSPIRE].

[20] T.W. Baumgarte and S.L. Shapiro, *On the numerical integration of Einstein's field equations*, *Phys. Rev.* **D 59** (1999) 024007 [gr-qc/9810065] [INSPIRE].

[21] E. Bentivegna and I. Hinder, *Accurate measurement of length scaling in S^3 black-hole lattices*, in preparation.

[22] E. Schnetter, S.H. Hawley and I. Hawke, *Evolutions in 3D numerical relativity using fixed mesh refinement*, *Class. Quant. Grav.* **21** (2004) 1465 [gr-qc/0310042] [INSPIRE].

[23] R.M. Wald, *General relativity*, The University Of Chicago Press, Chicago and London (1984).

[24] D.A. Nichols et al., *Visualizing Spacetime Curvature via Frame-Drag Vortexes and Tidal Tendexes I. General Theory and Weak-Gravity Applications*, *Phys. Rev.* **D 84** (2011) 124014 [arXiv:1108.5486] [INSPIRE].

[25] J.A. Valiente Kroon, *A Characterisation of Schwarzschildean initial data*, *Phys. Rev.* **D 72** (2005) 084003 [gr-qc/0504003] [INSPIRE].

JCAP08(2015)025